Chemical Science

ROYAL SOCIETY OF CHEMISTRY

EDGE ARTICLE

View Article Online
View Journal | View Issue

Cite this: *Chem. Sci.*, 2023, **14**, 8897

All publication charges for this article have been paid for by the Royal Society of Chemistry

Received 6th April 2023
Accepted 20th July 2023

DOI: 10.1039/d3sc01786a

rsc.li/chemical-science

Photocontrolled activation of doubly *o*-nitrobenzyl-protected small molecule benzimidazoles leads to cancer cell death†

Manzoor Ahmad, ‡[a] Naveen J. Roy, [a] Anurag Singh,§[a] Debashis Mondal, ¶[a] Abhishek Mondal, [a] Thangavel Vijayakanth, [b] Mayurika Lahiri [c] and Pinaki Talukdar *[a]

Artificial biomimetic chloride anionophores have shown promising applications as anticancer scaffolds. Importantly, stimuli-responsive chloride transporters that can be selectively activated inside the cancer cells to avoid undesired toxicity to normal, healthy cells are very rare. Particularly, light-responsive systems promise better applicability for photodynamic therapy because of their spatiotemporal controllability, low toxicity, and high tunability. Here, in this work, we report *o*-nitrobenzyl-linked, benzimidazole-based singly and doubly protected photocaged protransporters **2a**, **2b**, **3a**, and **3b**, respectively, and benzimidazole-2-amine-based active transporters **1a–1d**. Among the active compounds, *trifluoromethyl*-based anionophore **1a** showed efficient ion transport activity (EC_{50} = 1.2 ± 0.2 μM). Detailed mechanistic studies revealed Cl^-/NO_3^- antiport as the main ion transport process. Interestingly, double protection with photocages was found to be necessary to achieve the complete "OFF-state" that could be activated by external light. The procarriers were eventually activated inside the MCF-7 cancer cells to induce phototoxic cell death.

Introduction

Naturally occurring chloride transporters like prodigiosin, tambjamine, *etc.* are known to perturb the chloride ion homeostasis inside the cancer cells to induce apoptosis.[1,2] A wide variety of synthetic analogs in the form of ion channels and ion carriers have been developed that mimic natural systems and can lead cancer cells to undergo apoptosis.[3–8] However, the undesired cytotoxicity towards the normal, healthy cells is one of the drawbacks associated with most of these ion transport systems, due to the lack of their selectivity towards the cancer cells. Various stimuli-responsive ion transporters have been reported to overcome this issue where external stimuli are used to activate them. The different kinds of stimuli that have been utilized include pH,[9,10] light,[11] voltage,[12] ligand,[13,14] enzymes,[15–17] redox,[18–20] *etc.* However, very few stimuli-responsive systems have actually been activated inside the cancerous cells,[21,22] and hence, efficient systems with better therapeutic applications are needed. Light is one of the versatile stimuli that has been employed because of the unique combination of features of spatiotemporal control, remote addressability, extreme tunability, and biocompatibility.[23] The different photosystems that have been used to generate light-responsive ion transport systems include the use of photoswitches like azobenzene, acylhydrazone, phenylhydrazone, stiff-stilbene, *etc.*,[24–34] and photocages, *e.g.*, *o*-nitrobenzyl.[35,36] It is still a challenging task to design photoresponsive ion transport systems possessing a fully inactive 'OFF' state and a fully active 'ON' state. One promising approach to achieve this involves the use of photocleavable groups connected to block the anion binding sites in the active ion transporters that can be removed using external electromagnetic radiation. The *o*-nitrobenzyl (ONB) group is one such kind of photocage that has been utilized for the activation or delivery of anticancer drugs.[37–39] Our group demonstrated the photoactivation of ONB-linked indole-2-carboxamide-based procarriers inside the cancer cells to induce phototoxic cell death.[40] The active transporter, however, itself did not show any cell death and hints that systems with

[a]*Department of Chemistry, Indian Institute of Science Education and Research Pune, Dr Homi Bhabha Road, Pashan, Pune 411008, Maharashtra, India. E-mail: ptalukdar@iiserpune.ac.in*

[b]*The Shmunis School of Biomedicine and Cancer Research, George S. Wise Faculty of Life Sciences, Tel Aviv University, Tel Aviv 6997801, Israel*

[c]*Department of Biology, Indian Institute of Science Education and Research Pune, Dr Homi Bhabha Road, Pashan, Pune 411008, Maharashtra, India*

† Electronic supplementary information (ESI) available. See DOI: https://doi.org/10.1039/d3sc01786a

‡ Present address: Chemistry Research Laboratory, Mansfield Road, Oxford, OX1 3TA, UK.

§ Present address: Université libre de Bruxelles (ULB), Ecole polytechnique de Bruxelles, Engineering Molecular NanoSystems, Avenue Franklin Roosevelt 50, 1050 Brussels, Belgium.

¶ Present address: Faculty of Chemistry, Biological and Chemical Research Centre, University of Warsaw, Zwirkii Wigury 101, Warsaw 02-089, Poland.

better biological activities need to be developed for improved therapeutic applications.

Benzimidazole is one of the interesting moieties that is known to bind anions through hydrogen bonding interactions and has been used for ion transport purposes.[41] A wide variety of benzimidazole-based anion transporters have shown potential anticancer applications.[42] Recently, our group developed pyridyl-linked benzimidazole-based HCl cotransporters that were found to have five-fold higher efficiency compared to prodigiosin (a naturally occurring HCl cotransporter), and exhibited significant Cl^- mediated cell death in MCF-7 breast cancer cells.[43]

Such findings prompted us to utilize this efficient ion transport moiety by selectively activating it inside the cancer cells without affecting the normal cells. Here, we developed ONB-linked benzimidazole-2-amine procarriers **2a**, **2b**, **3a**, and **3b** that were photoactivated inside the artificial liposomes and MCF-7 breast cancer cells. We used benzimidazole-2-amines **1a–1d** as the active transporters that were expected to interact with the anions through imidazole and amine N–H hydrogen bonding interactions (Fig. 1A). Furthermore, different substituents were connected to the aromatic ring in order to fine-tune the membrane permeability and binding affinity of these anion transporters.[7,44] We anticipated that protection of the anion binding N–H protons with a photoresponsive ONB group would render them inactive for anion transport in the lipid membrane.

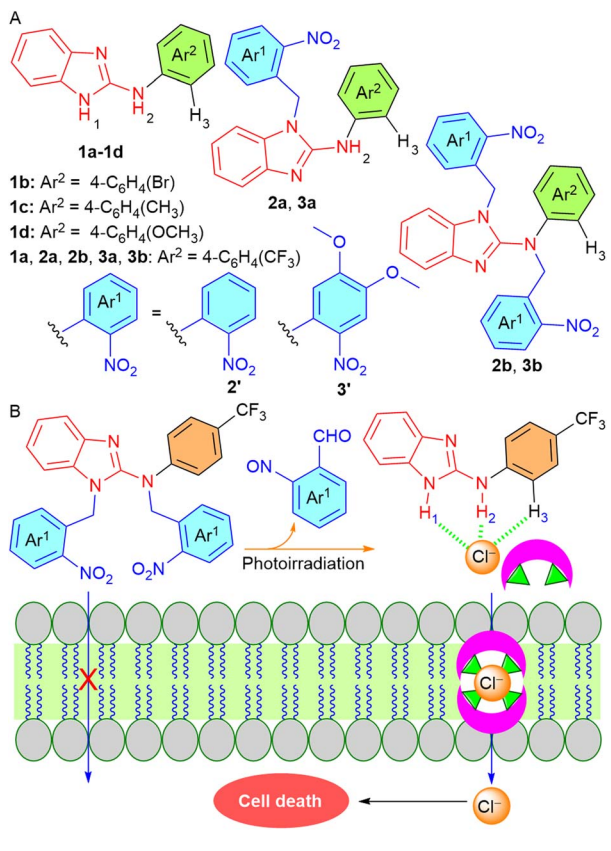

Fig. 1 (A) Chemical structures of the procarrier molecules **2a**, **2b**, **3a**, **3b** and active transporters **1a–1d**. (B) Working principle of photo-triggered activation inside the lipid membrane.

Eventually, the photocaged procarriers would be activated inside the artificial liposomes and cancer cells to induce cell death by utilizing external electromagnetic radiation (Fig. 1B). Moreover, the incorporation of methoxy groups into the ONB group was expected to affect the photolytic properties of the procarriers.[45]

Results and discussion

Synthesis

The synthesis of the active transporters **1a–1d** was achieved by reacting 2-chlorobenzimidazole **4** with different aromatic amines **5a–5d** in the presence of *p*-toluene sulfonic acid (Scheme 1). In order to synthesize the protected compounds **2a**, **2b**, **3a**, and **3b**, the most active transporter **1a** was coupled with the corresponding *o*-nitrobenzyl bromide derivatives **6a** and **6b**, respectively. The reaction of **1a** with one equivalent of **6a** and **6b** led to the formation of mono-ONB-protected compounds **2a** and **3a**, and on the other hand, the reaction of **1a** with the excess (3 equivalents) of **6a** and **6b** led to the formation of di-ONB protected compounds **2b** and **3b**, respectively. For the synthesis of the corresponding control compounds, 4-methoxyphenol **8** was reacted with the corresponding *o*-nitrobenzyl bromide derivatives **6a** and **6b** in the presence of potassium carbonate to furnish **9a** and **9b** in excellent yields.

Anion binding studies

After synthesizing compounds **1a–1d**, the chloride binding studies were performed by ^{1}H NMR titrations in acetonitrile-d_3 using TBACl (a Cl^- ion source). The addition of TBACl to the receptors led to a significant downfield shift of imidazole N–H_1, amine N–H_2, and (Ar)C–H_3 protons, indicating their involvement in the chloride binding through N–H$\cdots$$Cl^-$ and C(Ar)–H$\cdots$$Cl^-$ hydrogen bonding interactions (Fig. S22, S24, S26, and S28†). The Bindfit program[46] revealed 1 : 1 receptor : Cl^- binding stoichiometry and the binding constant values (K_a) were observed to be 2100 ± 185 M^{-1} for **1a**, 1200 ± 175 M^{-1} for **1b**, 500 ± 71 M^{-1} for **1c**, and 300 ± 43 M^{-1} for **1d**, respectively (Table 1, Fig. S23, S25, S27, and S29†). The evidence of 1 : 1 receptor : Cl^- binding stoichiometry was further clarified by electrospray ionization mass spectroscopic studies (ESI-MS). The data provided the peaks at m/z = 330.0620 and 332.0597, which correspond to the complex **1a**·Cl^- (Fig. S30†).

Ion transport studies

The ion transport properties of the compounds **1a–1d** were determined across egg yolk phosphatidylcholine unilamellar vesicles (EYPC-LUVs) entrapped with 8-hydroxy pyrene-1,3,6-trisulfonic acid trisodium salt (HPTS, a pH-sensitive dye) (EYPC-LUVs⊃HPTS) and 100 mM NaCl buffered at pH = 7.0.[47] Subsequently, a pH gradient was created across the vesicular membrane by adding NaOH to the extravesicular buffer. The dissipation of the pH gradient by the transporter molecules **1a–1d** was determined by monitoring the time-dependent change in the HPTS fluorescence (λ_{em} = 510 nm and λ_{ex} = 450 nm). Triton X-100 was added at the end of each experiment for calibration to get 100% transport activity. The ion transport activity

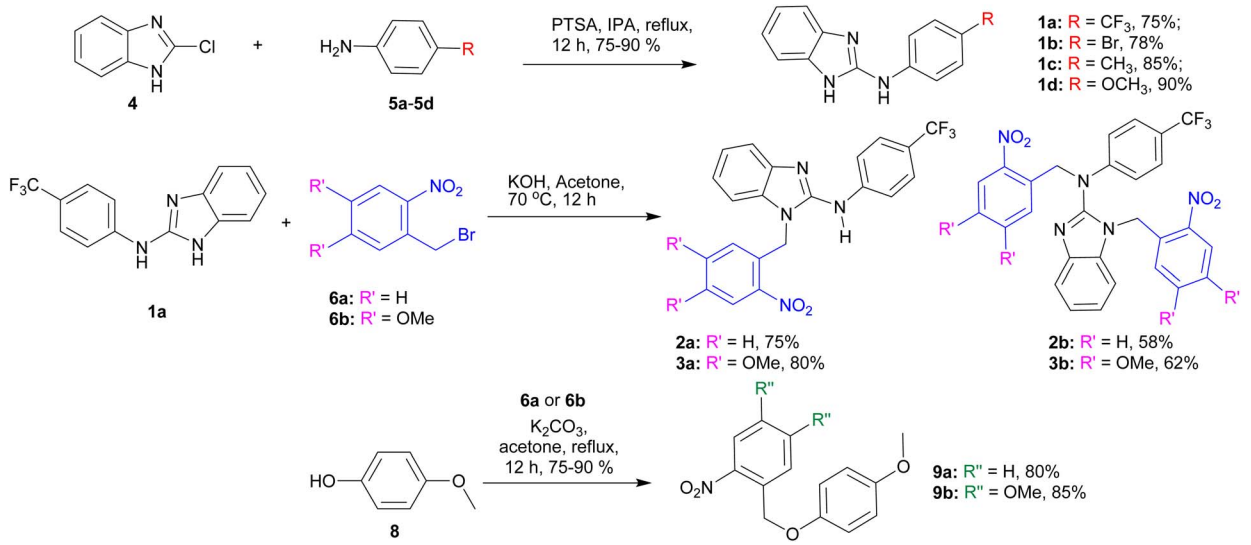

Scheme 1 Synthesis of active carriers **1a–1d**, ONB-protected procarriers **2a**, **2b**, **3a**, and **3b**, and control compounds **9a** and **9b**.

Table 1 Summary of log*P*, chloride binding K_a (M^{-1}) EC_{50} (μM), and Hill coefficient (*n*) values of compounds **1a–1d**

Comp	R	log*P*	K_a[a] (M^{-1})/Cl^-	EC_{50}[b] (μM)	*n*[c]
1a	CF_3	4.26	2100 ± 185	1.2 ± 0.2	2.3 ± 0.3
1b	Br	4.15	1200 ± 75	3.2 ± 0.2	2.0 ± 0.2
1c	CH_3	3.90	500 ± 71	13.5 ± 2.5	1.9 ± 0.6
1d	OCH_3	3.23	300 ± 43	26.9 ± 3.8	2.9 ± 0.8

[a] Association constants obtained using the Bindfit Program based on the 1 : 1 binding model for NH_2 protons. [b] Effective concentration to reach 50% of maximal activity across EYPC-LUVs entrapped with 1 mM HPTS, NaCl (100 mM), buffered at pH 7.0 using 10 mM HEPES. [c] Hill coefficient. log*P* values were calculated using MarvinSketch software.

monitored at $c = 7.5$ μM showed the ion transport sequence of **1a** > **1b** > **1d** > **1c** (Fig. 2A). The Hill analysis of the dose–response curves furnished the EC_{50} values (effective concentration to reach the 50% activity) of 1.2 ± 0.2 μM (1.9 mol%) for **1a**, 3.2 ± 0.2 μM (5.1 mol%) for **1b**, 13.5 ± 2.5 μM (21.6 mol%) for **1c**, and 26.9 ± 3.8 μM (43.0 mol%) for **1d**, respectively (Fig. S32–S35†). The Hill coefficient of ~2 suggests the involvement of two receptor molecules to drive the ion transport across the lipid membrane. Furthermore, upon varying the cations in the external buffer by using different MCl salt solutions ($M^+ = Li^+$, Na^+, K^+, Rb^+, and Cs^+), no significant change in the ion transport rate was observed, indicating no role of cations in the transport process (Fig. S37†). However, upon varying the anions in the external buffer by using different NaX salts ($X = Cl^-$, Br^-, I^-, ClO_4^-, and NO_3^-), a significant change in the ion transport was observed, indicating the active role of anions in the transport process (Fig. 2B).

Chloride leakage studies

The Cl^- leakage for **1a** was monitored across lucigenin-based vesicles. Vesicles were prepared by entrapping lucigenin dye (1 mM) in 100 mM $NaNO_3$ buffered at pH 7.0.[48] Subsequently, a Cl^-/NO_3^- gradient was created by adding a Cl^- pulse in the external buffer, and the transport of Cl^- ions was determined by measuring the time-dependent change in the lucigenin fluorescence ($\lambda_{ex} = 455$ nm and $\lambda_{em} = 535$ nm). The concentration-dependent fluorescent study of **1a** is shown in Fig. 2C. Hill analysis of the dose–responsive curve furnished the EC_{50} value of 13.9 ± 3.5 μM (Fig. S39†).

Ion selectivity and mechanism of ion transport

Mechanistically speaking, the ion transport in the above studies can occur through one of the modes of (a) H^+/X^- symport, (b) OH^-/X^- antiport, (c) H^+/M^+ antiport, or (d) OH^-/M^+ symport. However, no change in the ion transport activity in the presence of cations in the HPTS-based studies rules out the possibilities of H^+/M^+ antiport and OH^-/M^+ symport modes. To validate the antiport mode, the chloride efflux of **1a** across LUVs containing 500 mM of KCl and suspended in a 500 mM potassium gluconate solution was monitored in the presence and absence of valinomycin (highly selective K^+ antiporter) and monensin (an H^+/K^+ antiporter) using a chloride sensitive ion-selective electrode (Fig. 2E). A significant enhancement in the chloride efflux was observed in the presence of valinomycin (Fig. 2F), while on the other hand, no change was observed in the presence of monensin (Fig. 2G). This cooperative effect of valinomycin and **1a** is a proof of the antiport mode of ion transport.[49–51]

Additionally, the classic U-tube experiment was performed to confirm the carrier mode of ion transport. Significant chloride transport from the source arm of the U-tube was observed into the receiver arm only in the presence of the transporter molecule **1a** (Fig. 2D), which indicates the carrier mode of ion transport.[52–54]

Geometry optimization and binding energy calculation

To obtain insights into the geometry of the $[(\mathbf{1a})_2{+}Cl^-]$ complex, DFT calculations were performed. The $[(\mathbf{1a})_2{+}Cl^-]$ complex was

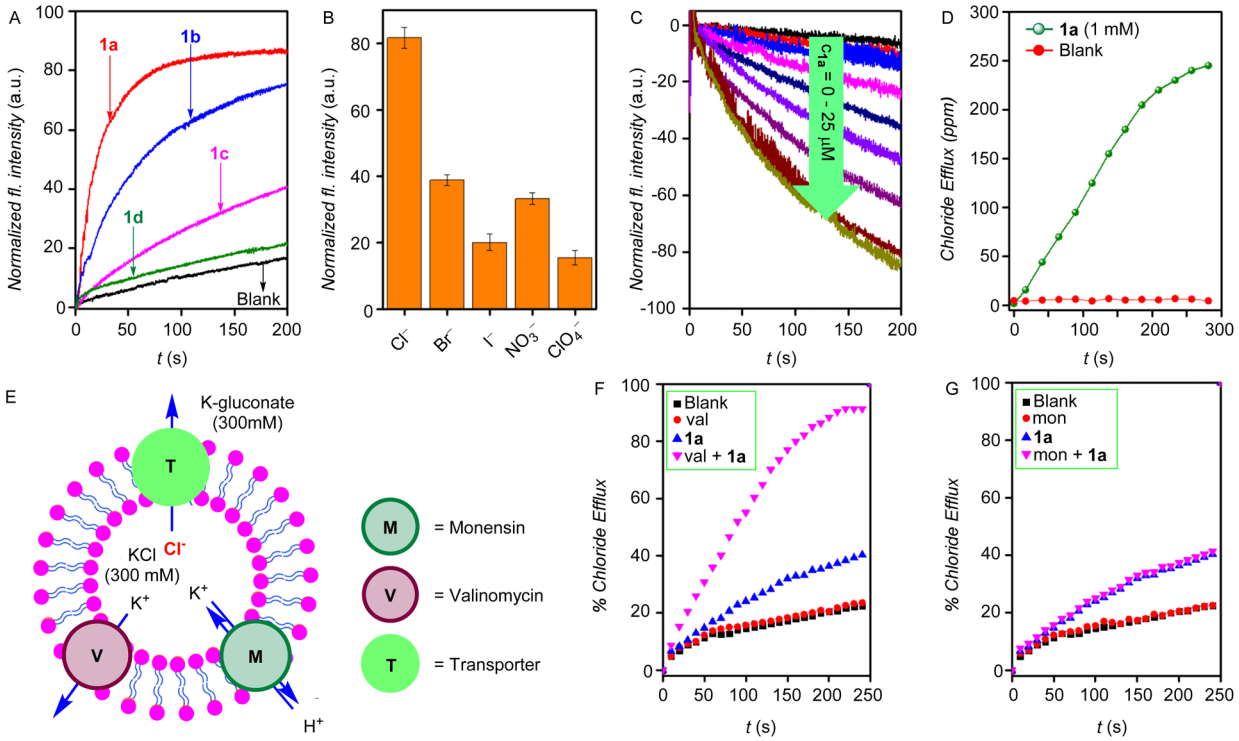

Fig. 2 (A) Activity comparison of **1a–1d** (7.5 μM) across EYPC–LUVs⊃HPTS. (B) Anion selectivity of **1a** (5.0 μM) by varying external anions across EYPC–LUVs⊃HPTS, each bar graph represents mean ion transport activity, calculated from three independent experiments. (C) Concentration-dependent activity of compound **1a** across EYPC–LUVs⊃Lucigenin. (D) The chloride transport in the U-tube experiment in the presence and absence of transporter molecule **1a**. (E) Schematic representation of ISE-based valinomycin and monensin assays. Normalized chloride efflux of **1a**, (F) in the presence and absence of monensin, and (G) the presence and absence of valinomycin.

chosen based on the experimentally determined Hill coefficient value, which was found to be ~2, indicating that two receptor molecules are involved in the formation of an active complex during the ion transport process. Initially, the CONFLEX 8 software program[55,56] provides several conformational structures with almost equal populations (Fig. S51†). The highest Boltzmann populated structure was then optimized using the Gaussian 09 program[57] utilizing a B3LYP functional and 6-31G (d, p) basis set.[58] The geometry-optimized analysis of the [(**1a**)$_2$+Cl$^-$] complex showed the involvement of two receptor molecules interacting orthogonally with the chloride anion interacting through benzimidazole-N–H$_1$···Cl$^-$ (H$_1$···Cl$^-$ = 2.312 Å), amine-N–H$_2$···Cl$^-$ (H$_2$···Cl$^-$ = 2.274 Å), and C(Ar)–H$_3$···Cl$^-$ (H$_3$···Cl$^-$ = 3.620 Å) hydrogen bonding interactions (Fig. 3E). The binding energy was predicted to be −68.46 kcal mol^{-1}.

Photolytic studies

After successfully achieving the ion transport studies, the photolytic studies of the procarriers **2a**, **2b**, **3a**, and **3b** were performed. Initially, The UV-Vis absorption studies of these compounds were performed in acetonitrile. The absorption spectra of all compounds were found to be extended up to 400 nm of wavelength with strong absorption bands at λ = 350 nm for dimethoxy-ONB substituted compounds **3a** and **3b** compared to the weaker absorption bands for the compounds **2a** and **2b**, respectively (Fig. 3A). After UV-Vis absorption studies, the photolytic studies were performed through ^{1}H NMR analysis. Initially, the ^{1}H NMR spectrum of each of the procarriers was recorded in DMSO-d_6. Subsequently, each sample was subjected to photoirradiation at 400 nm using LEDs (1 × 3.8 Watt) at different time intervals, and the ^{1}H NMR spectrum was recorded after each photoirradiation process. Finally, ^{1}H NMR spectra of procarrier molecules (**2a**, **2b**, **3a**, and **3b**) before irradiation, photoirradiated samples, and as-synthesized active carrier **1a** were stacked (Fig. S43–S45†). The photoirradiation process of compound **3b** is shown in Fig. 3B. Upon photoirradiation, H$_c$ and H$_d$ protons corresponding to the ONB group of the procarriers at 5.52 ppm and 5.31 ppm disappeared with the appearance of a new signal at 12.01 ppm corresponding to proton H$_e$ of the *o*-nitrosobenzaldehyde byproduct **10b**. Similarly, new proton signals H$_a$ and H$_b$ appeared at 11.11 ppm and 9.92 ppm, respectively, which correspond to the proton signals of as-synthesized benzimidazole carrier **1a**. These changes in the ^{1}H NMR spectrum of the **3b** upon photoirradiation confirmed the release of the active transporter **1a** along with the *o*-nitrosobenzaldehyde byproduct **11**. Similarly, compounds **2a**, **2b**, and **3a** furnish the formation of active transporter **1a** and the *o*- nitrosobenzaldehyde byproducts **10a** and **10b**, respectively. Noticeably, the dimethoxy-based compounds **3a** and **3b** showed efficient photocleavage (20 minutes for complete deprotection) as compared to the corresponding simple ONB-

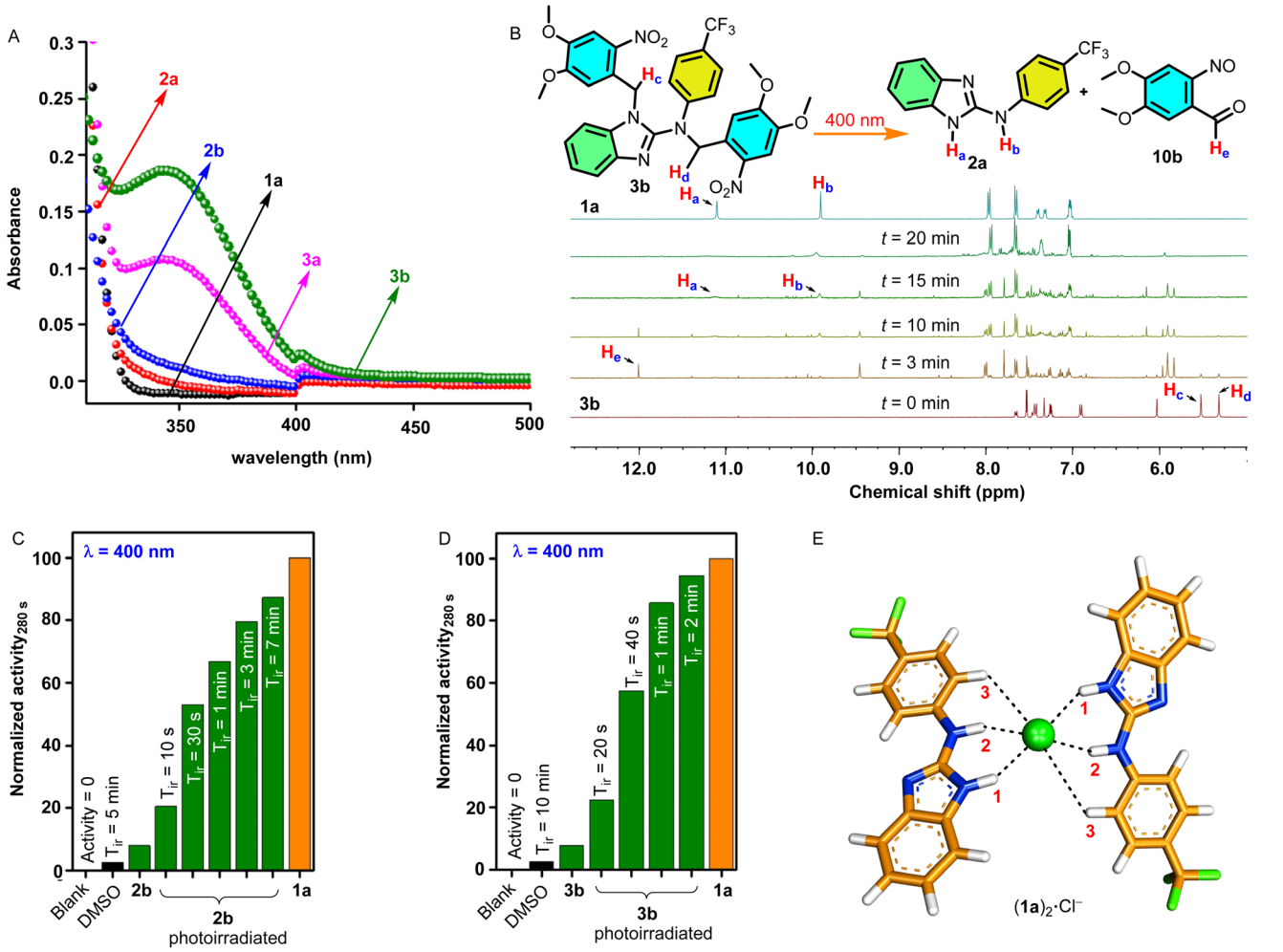

Fig. 3 (A) UV-Visible absorption spectra of **1a** and ONB-protected procarrier compounds **2a**, **2b**, **3a**, and **3b**. (B) Phototriggered release of an active carrier **1a** from ONB-protected procarrier **3b** monitored by ^{1}H NMR studies recorded in DMSO-d_6 photoirradiated using a 400 nm LED at different time intervals. Normalized ion transport activity data upon photoirradiation at 400 nm for (C) **2b** and (D) **3b**, respectively. (E) The geometry-optimized structure of the [(**1a**)$_2$+Cl$^-$] complex.

based compounds **2a** and **2b** (40 minutes for complete deprotection).

Photocleavable ion transport studies

Soon after the photolytic studies, the phototriggered ion transport studies were carried out, across HPTS entrapped EYPC-LUVs. Initially, the ion transport activities for the protected compounds **2a**, **2b**, **3a**, and **3b** were monitored. Subsequently, the vesicles containing these compounds were photoirradiated at different time intervals using a LED of 400 nm wavelength, and ion transport activity was monitored after each photoirradiation process. The ion transport activity after the photoirradiation process was compared with that of the as-synthesized active transporter **1a**. The ion transport activity of the blank (only with DMSO) was taken as 0%, and for active transporter **1a** as 100%. The procarriers **2b** and **3b** showed excellent enhancement in the ion transport activity upon photoirradiation (Fig. 3C and D), and on the other hand, compounds **2a** and **3a** did not furnish any change in the transport activity before and after the photoirradiation (Fig. S49†). These results indicate that the protection of both imidazole N–H and amine N–H protons is necessary to render the procarrier molecules inactive that are then successfully activated using external electromagnetic radiation. In the monoprotected compounds (**2a** and **3a**), the amine N–H$_2$ and the aryl C–H$_3$ protons (Fig. 1A) are capable of cooperatively binding to the anion. Hence **2a** and **3a** exhibited substantial ion transport activity through probably the formation of transport complexes with the anion involving single or multiple host molecules. In the case of the doubly protected **2b** and **3b**, the absence of both benzimidazole (N–H$_1$) and amine (N–H$_2$) protons renders them incapable of anion transport as the aryl (C–H$_3$) proton alone offers very weak anion binding and transport. The vesicles containing only DMSO did not furnish any transport activity while applying the photoirradiation for 10 min, confirming that light does not disrupt the integrity of the lipid membrane. Furthermore, the dimethoxy-ONB-based procarrier **3b** furnishes efficient photoactivation (complete

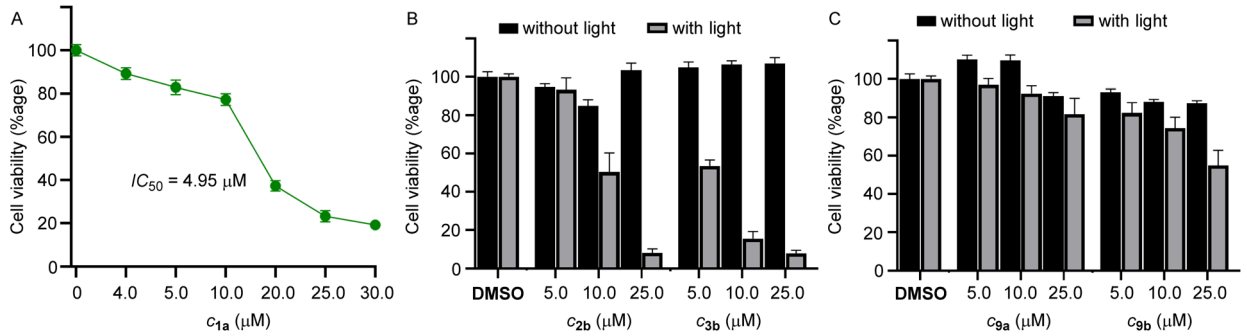

Fig. 4 (A) Dose-dependent cell viability of MCF-7 cells incubated with **1a** (0–25 μM each) for 24 hours. (B) Cell viability obtained from the MTT assay upon addition of **2b** and **3b** for 24 h in MCF-7 cells in the absence of light and upon photoirradiation at 400 nm for 20 min using (1 × 3.8 W LED). Mean cell viability was obtained from three independent experiments. (C) Cell viability obtained from the MTT assay upon addition of **9a** and **9b** for 24 h in MCF-7 cells in the absence of light and upon photoirradiation at 400 nm for 20 min using (1 × 3.8 W LED). Mean cell viability was obtained from three independent experiments.

activation within 2 min of photoirradiation) compared to simple ONB-based procarrier **2b** (complete activation after 7 min of photoirradiation) due to the photolytic properties of dimethoxy-based ONB systems as evident from NMR (Fig. 3B, S46†) and vesicle transport (Fig. 3C and D) studies.

Cellular viability and phototriggered cell death

Among the compounds **1a–1d**, we chose **1a** for the biological studies because of its efficient ion transport properties. The MCF-7 cells (human breast cancer cell line) were incubated with **1a** (0–25 μM) for 24 h, and cell viability was monitored using the standard MTT assay.[59] The compound furnished efficient cytotoxicity with an IC_{50} value of 4.5 μM (Fig. 4A).

Subsequently, for phototriggered cell death, MCF-7 cells were incubated with procarriers **2b** and **3b**, respectively, in two different 96-well plates. One of the plates containing the pro carriers **2b** and **3b** was photoirradiated at 400 nm (1 × 3.8 W LED, 20 min), and other plates containing the same compounds were not photoirradiated in order to observe the effect of photoirradiation in the cytotoxicity process. The cell plates were then kept in the incubator for 24 h and monitored using the standard MTT assay. Photoirradiation leads to significant cell death, likely due to the formation of the active transporter **1a** (Fig. 4B). Cells that do not contain the procarrier molecules do not furnish any cell death, which indicates that cells are not destroyed by light. Furthermore, in order to analyze the effect of *in situ* generated *o*-nitrosobenzaldehyde byproducts **10a** and **10b**, control compounds **9a** and **9b** were used. These compounds generate the same byproduct upon photoirradiation as is generated by the photoirradiation of procarrier compounds **2b** and **3b**. Photoirradiation of these control compounds did not furnish any significant cytotoxicity, which rules out any role of the nitrobenzaldehyde byproducts in the cytotoxicity process (Fig. 4C).

Conclusions

In conclusion, we developed benzimidazole amine-based active anionophores **1a–1d** and doubly protected ONB-linked photocaged procarriers **2b** and **3b**, respectively. The chloride binding studies of receptors were confirmed by ^{1}H NMR titration and ESI-MS studies. Among different active compounds, *trifluoromethyl*-based anionophore **1a** showed efficient ion transport activity with an EC_{50} value of 1.2 ± 0.2 μM. The Hill coefficient was found to be ~2, which indicates the involvement of two receptor molecules in driving the ion transport process. Detailed mechanistic studies confirmed Cl^-/NO_3^- antiport as the primary ion transport process. The double protection of the active anionophore **1a** with ONB-based photocages to give procarriers **2b** and **3b** renders them inactive due to the blockage of anion-binding sites. These procarriers were photoactivated inside the artificial liposomes using external electromagnetic radiation of 400 nm. Eventually, the photoactivation of the procarriers **2b** and **3b** inside the MCF-7 cancer cells leads to photoinduced cell death.

Data availability

The authors declare that all data supporting the findings of this study are available within the article and ESI,† and raw data files are available from the corresponding author upon request.

Author contributions

P.T. conceived the project and directed the experimental studies. N. J. R. performed the biological studies. A. S. performed the anion binding studies. M. A. synthesized and characterized the compounds, and performed the ion transport studies. D. M. performed the computational studies. A. M. performed photoirradiation studies. T. V. performed the characterization of some of the compounds. M. A. and P. T. wrote the paper. All authors approved the final version of the manuscript.

Conflicts of interest

There are no conflicts to declare.

Acknowledgements

This work was supported by the Science and Engineering Research Board (SERB), Govt. of India (EMR/2016/001897, DIA/

2018/000017), and Department of Biotechnology (DBT), Govt. of India (BT/HRD/NBA/38/06/2018). M. A. and D. M. thank UGC, Govt. of India for research fellowships. N. J. R. thanks CSIR, Govt. of India for a research fellowship. A. S. thanks DST-Inspire for the fellowship. A. M. thanks IISER Pune and Prime Minister's Research Fellowship.

References

1 S. Cheung, D. Wu, H. C. Daly, N. Busschaert, M. Morgunova, J. C. Simpson, D. Scholz, P. A. Gale and D. F. O'Shea, *Chem*, 2018, **4**, 879–895.
2 J. L. Sessler, L. R. Eller, W. S. Cho, S. Nicolaou, A. Aguilar, J. T. Lee, V. M. Lynch and D. J. Magda, *Angew. Chem., Int. Ed.*, 2005, **44**, 5989–5992.
3 T. Saha, M. S. Hossain, D. Saha, M. Lahiri and P. Talukdar, *J. Am. Chem. Soc.*, 2016, **138**, 7558–7567.
4 S.-K. Ko, S. K. Kim, A. Share, V. M. Lynch, J. Park, W. Namkung, W. Van Rossom, N. Busschaert, P. A. Gale, J. L. Sessler and I. Shin, *Nat. Chem.*, 2014, **6**, 885.
5 N. Busschaert, S.-H. Park, K.-H. Baek, Y. P. Choi, J. Park, E. N. W. Howe, J. R. Hiscock, L. E. Karagiannidis, I. Marques, V. Félix, W. Namkung, J. L. Sessler, P. A. Gale and I. Shin, *Nat. Chem.*, 2017, **9**, 667–675.
6 T. Saha, A. Gautam, A. Mukherjee, M. Lahiri and P. Talukdar, *J. Am. Chem. Soc.*, 2016, **138**, 16443–16451.
7 N. Busschaert, M. Wenzel, M. E. Light, P. Iglesias-Hernández, R. Pérez-Tomás and P. A. Gale, *J. Am. Chem. Soc.*, 2011, **133**, 14136–14148.
8 S. J. Moore, C. J. E. Haynes, J. González, J. L. Sutton, S. J. Brooks, M. E. Light, J. Herniman, G. J. Langley, V. Soto-Cerrato, R. Pérez-Tomás, I. Marques, P. J. Costa, V. Félix and P. A. Gale, *Chem. Sci.*, 2013, **4**, 103–117.
9 E. N. W. Howe, N. Busschaert, X. Wu, S. N. Berry, J. Ho, M. E. Light, D. D. Czech, H. A. Klein, J. A. Kitchen and P. A. Gale, *J. Am. Chem. Soc.*, 2016, **138**, 8301–8308.
10 S. V. Shinde and P. Talukdar, *Angew. Chem., Int. Ed.*, 2017, **56**, 4238–4242.
11 L. Lien, D. C. J. Jaikaran, Z. Zhang and G. A. Woolley, *J. Am. Chem. Soc.*, 1996, **118**, 12222–12223.
12 Y. Kobuke and K. Morita, *Inorg. Chim. Acta*, 1998, **283**, 167–174.
13 M. M. Tedesco, B. Ghebremariam, N. Sakai and S. Matile, *Angew. Chem., Int. Ed.*, 1999, **38**, 540–543.
14 P. Talukdar, G. Bollot, J. Mareda, N. Sakai and S. Matile, *Chem.–Eur. J.*, 2005, **11**, 6525–6532.
15 Y. R. Choi, B. Lee, J. Park, W. Namkung and K.-S. Jeong, *J. Am. Chem. Soc.*, 2016, **138**, 15319–15322.
16 E. B. Park and K.-S. Jeong, *Chem. Commun.*, 2015, **51**, 9197–9200.
17 N. Akhtar, N. Pradhan, A. Saha, V. Kumar, O. Biswas, S. Dey, M. Shah, S. Kumar and D. Manna, *Chem. Commun.*, 2019, **55**, 8482–8485.
18 A. Docker, T. G. Johnson, H. Kuhn, Z. Zhang and M. J. Langton, *J. Am. Chem. Soc.*, 2023, **145**, 2661–2668.
19 M. Fares, X. Wu, D. Ramesh, W. Lewis, P. A. Keller, E. N. W. Howe, R. Pérez-Tomás and P. A. Gale, *Angew. Chem., Int. Ed.*, 2020, **59**, 17614–17621.
20 B. Zhou and F. P. Gabbaï, *Chem. Sci.*, 2020, **11**, 7495–7500.
21 S. B. Salunke, J. A. Malla and P. Talukdar, *Angew. Chem., Int. Ed.*, 2019, **58**, 5354–5358.
22 J. A. Malla, R. M. Umesh, S. Yousf, S. Mane, S. Sharma, M. Lahiri and P. Talukdar, *Angew. Chem., Int. Ed.*, 2020, **59**, 7944–7952.
23 M. R. Banghart, M. Volgraf and D. Trauner, *Biochemistry*, 2006, **45**, 15129–15141.
24 R. F. Khairutdinov and J. K. Hurst, *Langmuir*, 2004, **20**, 1781–1785.
25 M. Ahmad, S. Metya, A. Das and P. Talukdar, *Chem.–Eur. J.*, 2020, **26**, 8703–8708.
26 A. Kerckhoffs and M. J. Langton, *Chem. Sci.*, 2020, **11**, 6325–6331.
27 Y. R. Choi, G. C. Kim, H.-G. Jeon, J. Park, W. Namkung and K.-S. Jeong, *Chem. Commun.*, 2014, **50**, 15305–15308.
28 M. Ahmad, S. Chattopadhayay, D. Mondal, T. Vijayakanth and P. Talukdar, *Org. Lett.*, 2021, **23**, 7319–7324.
29 W.-Z. Wang, L.-B. Huang, S.-P. Zheng, E. Moulin, O. Gavat, M. Barboiu and N. Giuseppone, *J. Am. Chem. Soc.*, 2021, **143**, 15653–15660.
30 Y. Zhou, Y. Chen, P.-P. Zhu, W. Si, J.-L. Hou and Y. Liu, *Chem. Commun.*, 2017, **53**, 3681–3684.
31 J.-Y. Chen and J.-L. Hou, *Org. Chem. Front.*, 2018, **5**, 1728–1736.
32 C. Wang, S. Wang, H. Yang, Y. Xiang, X. Wang, C. Bao, L. Zhu, H. Tian and D.-H. Qu, *Angew. Chem., Int. Ed.*, 2021, **60**, 14836–14840.
33 M. Ahmad, D. Mondal, N. J. Roy, T. Vijayakanth and P. Talukdar, *ChemPhotoChem*, 2022, **6**, e202200002.
34 T. G. Johnson, A. Sadeghi-Kelishadi and M. J. Langton, *J. Am. Chem. Soc.*, 2022, **144**, 10455–10461.
35 C. Bao, M. Ma, F. Meng, Q. Lin and L. Zhu, *New J. Chem.*, 2015, **39**, 6297–6302.
36 L. E. Bickerton and M. J. Langton, *Chem. Sci.*, 2022, **13**, 9531–9536.
37 S. K. Choi, M. Verma, J. Silpe, R. E. Moody, K. Tang, J. J. Hanson and J. R. Baker, *Bioorg. Med. Chem.*, 2012, **20**, 1281–1290.
38 W. S. Shin, J. Han, R. Kumar, G. G. Lee, J. L. Sessler, J.-H. Kim and J. S. Kim, *Sci. Rep.*, 2016, **6**, 29018.
39 N.-C. Fan, F.-Y. Cheng, J.-a. A. Ho and C.-S. Yeh, *Angew. Chem., Int. Ed.*, 2012, **51**, 8806–8810.
40 S. B. Salunke, J. A. Malla and P. Talukdar, *Angew. Chem., Int. Ed.*, 2019, **58**, 5354–5358.
41 C.-C. Peng, M.-J. Zhang, X.-X. Sun, X.-J. Cai, Y. Chen and W.-H. Chen, *Org. Biomol. Chem.*, 2016, **14**, 8232–8236.
42 X.-H. Yu, C.-C. Peng, X.-X. Sun and W.-H. Chen, *Eur. J. Med. Chem.*, 2018, **152**, 115–125.
43 A. Mondal, J. A. Malla, H. Paithankar, S. Sharma, J. Chugh and P. Talukdar, *Org. Lett.*, 2021, **23**, 6131–6136.
44 C. A. Lipinski, F. Lombardo, B. W. Dominy and P. J. Feeney, *Adv. Drug Deliv. Rev.*, 1997, **23**, 3–25.

45 M. J. Hansen, W. A. Velema, M. M. Lerch, W. Szymanski and B. L. Feringa, *Chem. Soc. Rev.*, 2015, **44**, 3358–3377.
46 **http://app.supramolecular.org/bindfit/**, accessed July 2017.
47 A. Roy, T. Saha, M. L. Gening, D. V. Titov, A. G. Gerbst, Y. E. Tsvetkov, N. E. Nifantiev and P. Talukdar, *Chem.–Eur. J.*, 2015, **21**, 17445–17452.
48 B. L. Schottel, H. T. Chifotides and K. R. Dunbar, *Chem. Soc. Rev.*, 2008, **37**, 68–83.
49 X. Wu, E. N. W. Howe and P. A. Gale, *Acc. Chem. Res.*, 2018, **51**, 1870–1879.
50 J. T. Davis, P. A. Gale and R. Quesada, *Chem. Soc. Rev.*, 2020, **49**, 6056–6086.
51 L. Chen, S. N. Berry, X. Wu, E. N. W. Howe and P. A. Gale, *Chem*, 2020, **6**, 61–141.
52 P. A. Gale, C. C. Tong, C. J. E. Haynes, O. Adeosun, D. E. Gross, E. Karnas, E. M. Sedenberg, R. Quesada and J. L. Sessler, *J. Am. Chem. Soc.*, 2010, **132**, 3240–3241.
53 D. Milano, B. Benedetti, M. Boccalon, A. Brugnara, E. Iengo and P. Tecilla, *Chem. Commun.*, 2014, **50**, 9157–9160.
54 N. Busschaert, I. L. Kirby, S. Young, S. J. Coles, P. N. Horton, M. E. Light and P. A. Gale, *Angew. Chem., Int. Ed.*, 2012, **51**, 4426–4430.
55 S. O. H. Goto, N. Nakayama and K. Ohta, *CONFLEX 8*, CONFLEX Corporation, Tokyo, Japan, 2012.
56 H. Goto and E. Osawa, *J. Am. Chem. Soc.*, 1989, **111**, 8950–8951.
57 M. J. Frisch, G. W. Trucks, H. B. Schlegel, G. E. Scuseria, M. A. Robb, J. R. Cheeseman, G. Scalmani, V. Barone, B. Mennucci, G. A. Petersson, H. Nakatsuji, M. Caricato, X. Li, H. P. Hratchian, A. F. Izmaylov, J. Bloino, G. Zheng, J. L. Sonnenberg, M. Hada, M. Ehara, K. Toyota, R. Fukuda, J. Hasegawa, M. Ishida, T. Nakajima, Y. Honda, O. Kitao, H. Nakai, T. Vreven, J. J. A. Montgomery, J. E. Peralta, F. Ogliaro, M. Bearpark, J. J. Heyd, E. Brothers, K. N. Kudin, V. N. Staroverov, T. Keith, R. Kobayashi, J. Normand, K. Raghavachari, A. Rendell, J. C. Burant, S. S. Iyengar, J. Tomasi, M. Cossi, N. Rega, J. M. Millam, M. Klene, J. E. Knox, J. B. Cross, V. Bakken, C. Adamo, J. Jaramillo, R. Gomperts, R. E. Stratmann, O. Yazyev, A. J. Austin, R. Cammi, C. Pomelli, J. W. Ochterski, R. L. Martin, K. Morokuma, V. G. Zakrzewski, G. A. Voth, P. Salvador, J. J. Dannenberg, S. Dapprich, A. D. Daniels, O. Farkas, J. B. Foresman, J. V. Ortiz, J. Cioslowski and D. J. Fox, *Gaussian 09, Revision D.01*, Gaussian, Inc., Wallingford CT, 2013.
58 A. D. McLean and G. S. Chandler, *J. Chem. Phys.*, 1980, **72**, 5639–5648.
59 J. A. Malla, R. M. Umesh, A. Vijay, A. Mukherjee, M. Lahiri and P. Talukdar, *Chem. Sci.*, 2020, **11**, 2420–2428.